DEVELOPMENT OF A METHOD FOR DETERMINING COMPLEX DIELECTRIC PERMITTIVITY AS AN INDICATOR OF ENERGY ABSORPTION IN SILVER NANOPARTICLE MODIFIED PHOTOVOLTAIC CONVERTERS

BORIS L. KRIT[1,3], MAROS SOLDAN[2], TATIANA Y. MOGILNAYA[1,4], SVETLANA I. SOLOMENNIKOVA[5], VLADIMIR V. KUVSHINOV[5], LEONID Y. YUFEREV[6], NATALYA V. MOROZOVA[3,4], BORIS A. YAKIMOVICH[5], NIKITA A. PETELIN[1], YAROSLAV V. DOLGUSHIN[1]

[1]Moscow Aviation Institute (National Research University), Moscow 125993, RF

[2]Slovak University of Technology in Bratislava, Faculty of Materials Science and Technology in Trnava, Institute of Integrated Safety, Slovakia

[3]Moscow State Technological University STANKIN, Moscow 127055, RF

[4]Moscow State Linguistic University, Moscow 119034, RF

[5]Sevastopol State University, Sevastopol 299053, Crimea

[6]Federal Scientific Agroengineering Center VIM, Moscow 109428, RF

DOI: 10.17973/MMSJ.2026_06_2026116

maros.soldan@stuba.sk

A nondestructive optical method for determining the complex dielectric permittivity ε(ω) of silicon photovoltaic converters (PVC) surfaces modified with silver nanoparticles is developed and experimentally validated. The method is based on backscattered radiation analysis and enables reconstruction of both real and imaginary components without altering the structure of objects under study [Kuric 2022]. Modified PVCs demonstrate a 2–5-fold increase in backscattering intensity and a 9–30% increase in photovoltaic pow er is observed, attributed to localized surface plasmon resonance. Compared to conventional ellipsometric approaches, the proposed method provides a simpler and robust alternative for in-situ diagnostics of plasmonic coatings. The obtained results indicate that the imaginary part of the dielectric permittivity plays a crucial role in determining the efficiency of electromagnetic energy absorption. The experimentally observed increase in photovoltaic power correlates with both the enhancement of the local electromagnetic field and the rise in effective dissipative losses in the near-surface region. Despite the theoretically predicted high absorption of electromagnetic energy, the overall efficiency gain of photovoltaic cells remains limited due to the localized nature of localized surface plasmon resonance, as well as scattering effects and structural inhomogeneity in the nanoparticle distribution.

KEYWORDS

silver nanoparticles, photovoltaic converters, complex dielectric permittivity, backscattering, plasmonics

1 INTRODUCTION

The development of advanced functional (“smart”) materials and coatings represents a key direction in modern materials science and technology, driven by the need to enhance performance without altering bulk properties. Such systems are typically classified as composite materials with structurally integrated functional components distributed either within the volume or at the surface, where their synergistic interaction determines the overall material response [Abu-Thabit 2020, Husain 2021, Grigoriev 2023, Mascenik 2024, Yelwa 2024].

In recent decades, the focus of materials engineering has shifted from extensive approaches toward surface modification strategies, collectively referred to as surface engineering. This approach enables targeted control of surface-dependent properties such as wear resistance, optical response, catalytic activity, and electrical behavior, while maintaining the integrity of the substrate [Suslov 2008, Ramezani 2023]. A particularly important trend is the incorporation of nanoscale features into material surfaces. Metallic nanoparticles (e.g., Ag, Au) deposited on semiconductor substrates, such as silicon, can significantly enhance light–matter interaction through plasmonic effects, resulting in improved optical absorption and increased efficiency of optoelectronic devices [Catchpole 2008, Yu 2017, Preston 2021, Gulyaev 2022, Krenicky 2024, Taha 2024, Parveen 2025].

In a number of our preceding works, we also presented experimental data showing that the deposition of silver nanoparticles on silicon photovoltaic converters (PVC) receiving surface causes a plasmonic resonance effect, which leads to an increase in electricity generation [Krit 2020, Mogilnaya 2021a,b]. A fundamental characteristic governing elect;omagnetic interaction with such materials is the complex dielectric permittivity, $\varepsilon = \varepsilon' + i\varepsilon''$. Accurate determination of dielectric properties is therefore essential for predicting the performance of functional coatings. However, the measurement of dielectric permittivity in nanostructured and multilayer coatings presents a significant challenge. Conventional techniques—including microwave resonators, impedance spectroscopy, transmission line methods, and time-domain reflectometry—all face limitations when applied to nanoscale systems [Chen 2004, Baker-Jarvis 1993, Krupka 2021, Schenk 2018].

One of the most widely used approaches for dielectric characterization is based on the determination of scattering parameters (S-parameters), as implemented in the Nicolson–Ross–Weir (NRW) method. While this technique is well established in the microwave domain, its application to optical frequencies is limited Objects

Silver-based nanostructures exhibit strong localized surface plasmon resonance (LSPR), enabling enhanced of the electromagnetic field configuration fixing and providing a basis for sensitive optical diagnostics. Despite these advantages, experimental determination of plasmon resonance parameters is constrained by angular limitations, optical losses, and boundary conditions. These limitations necessitate the development of advanced modeling approaches for reliable measurement of dielectric properties [Ordal 1983, Yang 2026, Kubota 2024, Mcoyi 2025].

Considering of the above, this paper aims to develop and test a method based on the analysis of electromagnetic radiation scattering to determine the complex dielectric constant. Unlike conventional optical characterization techniques such as ellipsometry, which require complicated instrumentation and

are sensitive to surface uniformity, the proposed method provides a nondestructive and experimentally accessible approach for retrieving complex dielectric permittivity based on backscattering analysis. This enables in-situ diagnostics of plasmonic coatings under realistic operating conditions.

2 MATERIALS AND METHODS

A total of 12 commercially produced silicon photovoltaic converters (PVC) were selected for the study. The selection procedure was performed in accordance with the methodology described in (Krit 2024). The external appearance and cross-sectional structure of the PVC are presented in Fig. 1. The architecture of the PVC consists of nine functional layers. Layers H1 and H2 form the contact grid, while layer H3 (~0.07 µm) acts as a transparent protective coating. The active layers responsible for photovoltaic conversion are H4–H6, and the silicon substrate surface is considered the primary functional interface. To ensure reproducibility and standardization of measurements, ten reference points were defined on the active surface of each PVC in regions free from metallization.

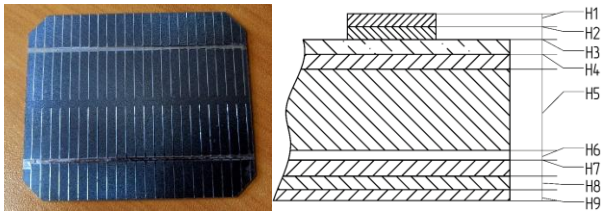

Figure 1. Photograph (a) and schematic cross-sectional view (b) of the PVC

Table 1. Parameters of the structural components of the PVC

Designation	Thickness (µm)	Conductivity type	Sheet resistance	Material (grade)
H1	0,7	-	-	POVI-0.5 solder
H2	2	-	-	M1 copper
H3	0,07	-	30-80	IN-2 indium
H4	0,7	N	50-80	orthophosphoric acid (OSCh 13-3)
H5	300	P	3-10	PSKKDB 3-10 silicon
H6	2	N	4-8	boric acid (OS413-4)
H7	0,05	-	-	VT1-00 titanium
H8	0,8	-	-	M1 copper
H9	0,7	-	-	POVI-0.5 solder

Silver nanoparticles were deposited onto the PVC surface using an electrochemical deposition system which was previously described in the paper [Mogilnaya 2021a] and is shown in Fig. 2. The PVC was placed in a cuvette with electrical contact provided by a stainless-steel cathode. The anode consisted of a metallic mesh electrode. A colloidal solution of silver nanoparticles was supplied into the system. Under the applied electric field, positively charged nanoparticles migrated and deposited onto the PVC surface. The system ensured continuous circulation of the solution.

The colloidal solution was synthesized by electro-pulse spark dispersion in distilled water. The resulting suspension contained Ag nanoparticles with a concentration of 50 mg/L and particle sizes in the range of 20–40 nm [Krit 2020).

The complex permittivity was determined based on measurements of electromagnetic radiation backscatter using a created special experimental setup, which will be described below.

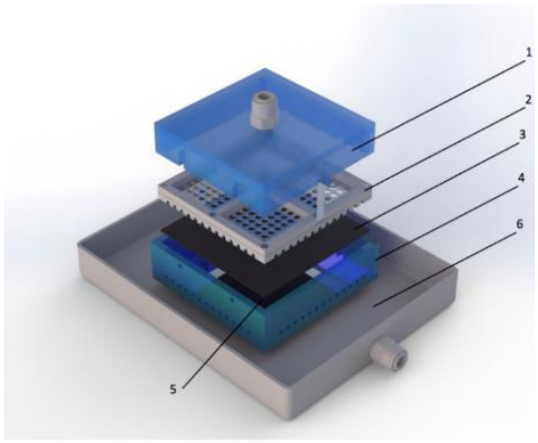

Figure 2. Scheme of the apparatus for silver nanoparticle deposition: (1) top clamping lid with inlet fitting, (2) top electrode in a Plexiglas frame, (3) PVC, (4) cuvette, (5) bottom electrode, (6) tray with outlet fitting

Electrical performance was evaluated by measuring the output power under open-circuit conditions using a digital multimeter Fluke 17B+. Illumination was provided by four halogen lamps (35 W). Measurements were conducted based on current–voltage characteristics in accordance with standard procedures [IEC 60904-1 2006].

Modeling of the Scattering Diagram

The evaluation of plasmon resonance conditions in Ag/Si nanostructures was performed using the Drude–Lorentz model. That approach allows estimation of angular positions of maximum reflected and scattered radiation.

Fig. 3 shows electron micrograph of samples after modification.

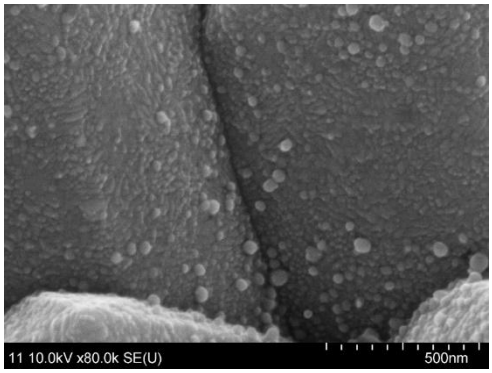

Figure 3. Electron micrograph of the modified PVC surface

The electron micrographs reveal that the nanoparticles are sparsely deposited on the substrate. These permits calculations using the simplified geometry shown in Fig. 4. In addition, the particles are nearly spherical (Fig. 3), which enables evaluation of the scattering diagram using the simplified model geometry [Mogilnaya 2020].

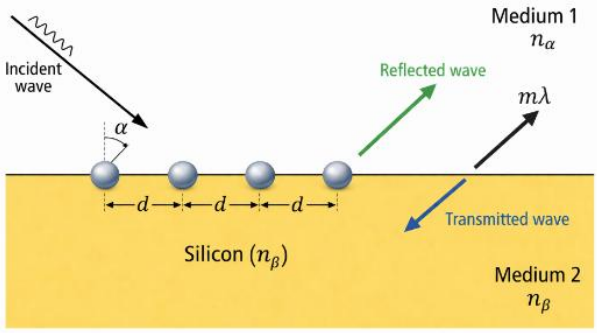

Figure 4. Schematic of the model geometry

The use of a simplified potential-based model (including elements of the Woods–Saxon formalism) is not intended for direct physical interpretation at the atomic scale, but rather

serves as an effective approximation for describing resonance behavior in confined nanoscale systems [Saga 2011, Schenk 2018]. This approach allows capturing the essential features of plasmonic response while maintaining analytical tractability.
The model is approximated as follows. A linearly polarized plane wave propagates through a medium with refractive index n_α and is incident on the surface at an angle α in the plane perpendicular to the grating. The dielectric material has a refractive index n_β, and the average distance between the nanoparticles is d.
The model calculates the transmission and reflection coefficients corresponding to refraction, specular reflection, and first-order diffraction.
The expression describing the field of a two-dimensional Gaussian beam in the paraxial approximation is as follows:

$$E_G(x,y) = E_0\sqrt{\frac{\omega_0}{\omega(y)}}\cdot e^{-(x/\omega(y))^2}\cdot exp\left(-i\left(ky-\eta(y)+\frac{kx^2}{2R(y)}\right)\right)e \quad (1)$$

is approximated by a plane-wave expansion:

$$Epw = \sum_{j=-Mk=0}^{M} * \sum_{j=-Mk=0}^{1} \alpha_{jk}\hat{u}_k(k_j)\cdot exp\left(-i(k_j\cdot r)\right) \quad (2)$$

where
each wave vector k_jpoints in a different direction specified by the index j;
a_jk is the amplitude, which takes different values for each wave vector and for each
of the two possible polarization directions associated with that wave vector (u^"kkj“ ʃ;
ω_0is the plasma frequency, and e is the electron charge.

Within this approximation, the response to the optical wave, independent of resonance type, can be obtained from the dielectric permittivity given by the Drude–Lorentz model [Car 2025]. The response to an optical wave at frequency ω can then be obtained from the expression for the dielectric permittivity of the skin layer at the material interfaces:

$$\varepsilon_r(\omega) = \varepsilon' + i\varepsilon'' \quad (3)$$

where ε_r (ω) is the complex dielectric permittivity of the skin layer;
ε^'and ε^''are the real and imaginary parts, respectively.

For plasmonic resonance, the spherical approximation [Zharova 2019] is adopted. In calculations of plasmonic phenomena, a nanoparticle consisting of N atoms can then be treated as a sphere of radius R=rN^(1/3), where r is the Wigner-Seitz radius and N is the number of atoms in the cluster. The Woods-Saxon potential can then be expressed as [Car 2025]:

$$U(r) = -\frac{U_0}{\exp\left[\frac{r-R}{a}\right]+1} \quad (4)$$

where U_0 is the depth of the potential well (a typical value of 50 MeV);
R=r_0 A^(1/3) is the nuclear radius (r_0≈1.25 fm is a parameter approximately equal to the average distance between nucleons in the nucleus;
A is the mass number of the nucleus), and a is the diffuseness parameter that characterizes the smearing of the potential well edge (a typical value of 0.5 fm).
The plasmonic resonance condition can be written as follows [Bohren 1983, Luukkonen 2011]:

$$R(\varepsilon'(\omega)+2\varepsilon_{rs}) = 0 \quad (5)$$

Since the particles are sufficiently separated, the field is treated as that produced by a single particle. In this case, the electric field distribution can be written as:

$$E(x,y,z) = \tilde{E}(x,y)e^{-ik_z z} \quad (6)$$

and the refractive index:

$$\epsilon_r = (n-ik)^2\ \sigma = 0\ \mu_r = 1 \quad (7)$$

the propagation equation, however, takes the following form:

$$\nabla\times(\nabla\times E) - k_0^2\epsilon_r E = 0. \quad (8)$$

In the resonance region, constructive interference occurs when the optical path difference between the two paths is an integer multiple of the vacuum wavelength, which is equivalent to the resonance condition:

$$m\lambda_0 = d\left(n_\beta \sin\beta_m - n_\alpha \sin\alpha\right) \quad (9)$$

where m=0,±1,±2,..., λ_0 is the vacuum wavelength, and β_m is the transmitted diffracted beam of order m.
For m=0, this reduces to refraction, as described by Snell's law:

$$\sin\alpha_0 = \sin\alpha \quad (10)$$

$$2\lambda_0 > dn_\alpha(1+|\sin\alpha|) \quad (11)$$

Since only first-order diffraction is considered in this work, the criterion for constructive interference—and consequently for resonance—is that the optical path difference between the two paths equals an integer multiple of the vacuum wavelength, or:

$$m\lambda_0 = dn_\alpha(\sin\alpha_m - \sin\alpha) \quad (12)$$

$$\sin\alpha_0 = \sin\alpha \quad (13)$$

$$2\lambda_0 > dn_\alpha(1+|\sin\alpha|) \quad (14)$$

Fig. 5 shows the backscattering coefficients as a function of the angle of incidence.

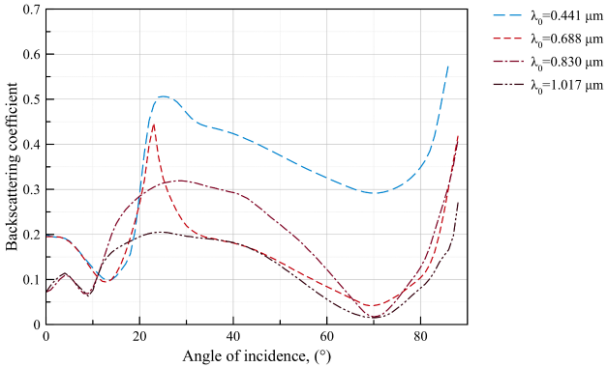

Figure 5. Backscattering coefficients as a function of the angle of incidence

These results indicate that resonance of the reflected radiation occurs for all wavelengths in the angular range of 20°–25°. This resonance enables a more accurate determination of the plate parameters. These findings are confirmed by our experimental studies [Tolmachev 2017, Zharova 2019, Saito 2021].

3 EXPERIMENTAL SETUP

The system is an optoelectronic platform based on coherent semiconductor laser sources (Fig. 6). A single-frequency laser module incorporating a distributed Bragg reflector (DBR) cavity ($\lambda \approx 0.635$–$0.685\ \mu$m) was used to generate a stable, well-collimated beam with low divergence, eliminating the need for additional alignment optics.
The laser source and photodetector were positioned at equal angles of incidence and detection (α=β), ensuring symmetric

measurement geometry. The setup provides precise control of the angular configuration and alignment among the source, sample, and detector.

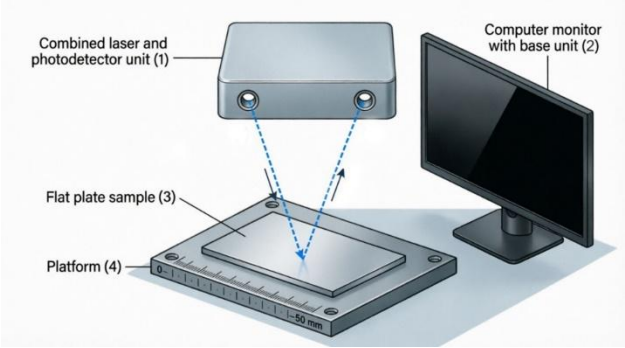

Figure 6. Schematic of the experimental measurement setup: (1) combined laser and photodetector unit, (2) computer monitor with base unit, (3) sample, (4) platform

The sample was mounted on a precision translation stage equipped with a micrometer-driven linear actuator along the optical axis. This configuration enabled controlled variation of the distance between the optical system and the sample. It is also facilitating analysis of the signal response near the reference position as well as evaluation of sensitivity and linearity.

Signal acquisition was performed using high-sensitivity, low-noise photodetectors optimized for the operating wavelength range. The system incorporates a power supply with independent channels, a control and processing unit, and a data acquisition interface.

Stabilization of the incident radiation intensity ensures that only the relative intensity of the backscattered signal is measured, thereby enabling accurate determination of the S_11 and S_21 parameters.

4 MEASUREMENT METHODOLOGY

According to [Kadochkin 2013], the effective refractive index (and consequently the complex dielectric permittivity) can be determined from the S-parameters (S_11 and S_21).

S_11 is the input reflection coefficient, defined as the ratio of the reflected signal amplitude from the substrate to the incident signal amplitude. S_21 is the transmission (or modified reflection) coefficient associated with the coated sample.

The measurement principle is illustrated in Figure 7. Laser radiation was directed onto selected regions of the bare substrate, and the backscattered signal was recorded to obtain S_11. Identical measurements were performed on samples coated with Ag nanoparticles to determine S_21, with the measurement positions kept the same through eucentric alignment.

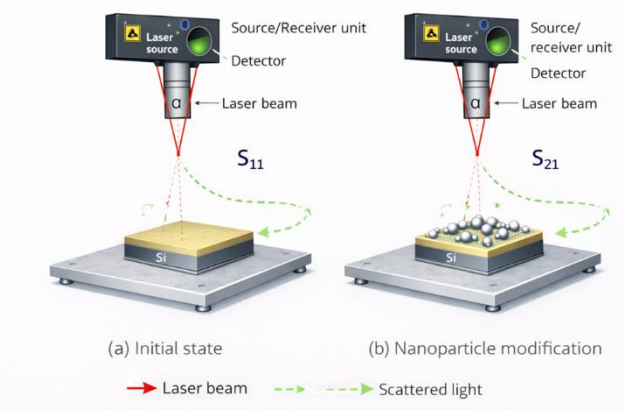

Figure 7. Schematic of the backscattering measurement principle

The permittivity is calculated using the formulas in [Luukkonen 2011] which demonstrates that the complex permittivity and complex magnetic permeability can be obtained from measured S-parameters after some mathematical transformations [Miglierini 2006]. Indeed, using the reflection coefficient from the boundary of a semi-infinite layer of material.

$$\varepsilon = \varepsilon_r \varepsilon_0 = (\varepsilon_r' - j\,\varepsilon_r'')\,\varepsilon_0. \tag{15}$$

$$\mu = \mu_r \mu_0 = (\mu_r' - j\,\mu_r'')\,\mu_0. \tag{16}$$

$$c = 1/\sqrt{\varepsilon_0 \mu_0} \tag{17}$$

$$\chi = \frac{S_{11}{}^2 - S_{21}{}^2 - \Gamma}{1-(S_{11}+S_{21})\Gamma'}. \tag{18}$$

$$\Gamma = \chi \pm \sqrt{\chi^2 - 1}. \tag{19}$$

$$\mathrm{n} = -\sqrt{\left[\frac{\mathrm{c}}{\omega d} ln(e^{\gamma d})\right]^2 + \left(\frac{\omega_c}{\omega}\right)^2} = -\sqrt{\left[\frac{\mathrm{c}}{\omega d} ln\left(\frac{S_{11}+S_{21}-\Gamma}{1-(S_{11}+S_{21})\Gamma'}\right)\right]^2 + \left(\frac{\omega_c}{\omega}\right)^2}. \tag{20}$$

$$n^2 = \varepsilon_r \mu_r = -\left[\frac{c}{\omega d}\ln(e^{\gamma d})\right]^2 + \left(\frac{\omega_c}{\omega}\right)^2. \tag{21}$$

$$\mu_r = \frac{1+\Gamma}{1-\Gamma}\sqrt{\frac{n^2-(\omega_c/\omega)^2}{1-(\omega_c/\omega)^2}}. \tag{22}$$

Where:

S11 - is the ratio of the amplitude of the signal reflected from the silicon substrate to the amplitude of the incoming signal;

S21 - is the reflectivity of the coated sample;

χ is the susceptibility of the medium;

Γ(ω) (Gamma function of frequency) is the complex frequency response, reflecting the frequency dependence of the system's response and including information about the amplitude and phase of the signal;

ω_c is the resonant frequency, corresponding to the laser frequency;

γ - is the attenuation/linewidth index, characterizing the resonance width and relaxation rate of the system;

ω_c/ω -is the deviation from the resonant frequency.

Since the S coefficients were determined using radiation from a single, highly stabilized source, calculation of these coefficients was reduced to measuring the intensities of the reflected signal with known laser parameters.

5 RESULTS AND DISCUSSION

Table 2 presents the averaged experimental values of backscattering intensity indicators for PVCs measured in the points not shielded by the contact grid (see Fig. 1), along with the corresponding values of complex dielectric permittivity calculated from these data. Additionally, the table includes the relative power increase (%) of converters modified with silver nanoparticles as compared to unmodified ones. These values were obtained from experimentally measured current–voltage characteristics.

It is well known that the real part of the complex dielectric permittivity (ε') of silicon is positive over a wide frequency range. However, under resonant conditions, when the frequency of incident radiation matches that of plasmonic excitations, the real part may become negative. In the present case, negative values of ε' indicate the presence of metallic nanoparticles on the surface and the possible presence of resonant phenomena.

In the visible and near-infrared spectral ranges, silver nanoparticles support localized surface plasmon resonances (LSPR). These resonances correspond to collective oscillations of conduction electrons, leading to strong enhancement of the local electromagnetic field near the particle surface and at the nanoparticle–silicon interface. This field enhancement increases the absorbed optical power density in the near-surface region of silicon, where electron–hole pair generation occurs which leads to an increase in energy production. Thus, the negative real part of the dielectric permittivity serves as a physical indicator of plasmonic resonance and assumes enhance in photoelectric conversion.

Table 2. Data of backscatter intensity and output increase measurements

PVC number	S_11	S_21	Emod\ Ecr	Complex dielectric permitivity	Power increase, %
1	83	260	3.13	ε= -14.695 + 0.564i	18.81
2	54	210	3.89	ε= -16.263 + 1.167i	29.63
3	23	80	3.48	ε= -11.779 + 0.593i	22.32
4	29	115	3.97	ε= -14.695 + 1.575i	30.14
5	32	123	3.84	ε= -16.263 + 1.033i	28.05
6	94	355	3.78	ε= -16.263 + 0.977i	28.63
7	23	65	2.83	ε= -16.263 + 0.347i	16.76
8	21	45	2.14	ε = -16.263 + 0.279i	12.94
9	39	136	3.49	ε = -16.263 + 0.599i	21.98
10	105	369	3.51	ε = -16.263 + 0.833i	23.45
11	22	42	1.91	ε= -14.626 + 0.229i	9.05
12	85	310	3.65	ε= -16.263 + 0.953i	27.96

Particular attention should be paid to the imaginary part of the complex dielectric permittivity (ε"), which characterizes the dissipative processes in the material. Positive values of ε" correspond to the effective absorption of scattered electromagnetic energy, the volumetric amount of which can be described by the classical expression [Bohren 1983]:

$$Q_{abs} = \frac{1}{2}\varepsilon_0 \omega \varepsilon''(\omega)|E|^2. \quad (23)$$

where ω is the angular frequency of incident radiation,
ε" is the imaginary part of the complex dielectric permittivity,
|E| is the amplitude of the local electric field.
According to the plasmonic absorption model for small metallic particles, excitation of localized surface plasmons leads to an additional strong enhancement of the local electric field intensity near the particle surface due to scattered electromagnetic radiation [Bohren 1983]. As a result, even moderate values of ε" can lead to a significant increase in absorbed power.
For silicon, at λ = 635 nm irradiation, the imaginary part of the complex dielectric constant was estimated using the optical constants (n, k). The calculation using the formula ε" = 2nk yielding ε" ≈ 0.147.
As follows from Table 2, the backscattering intensity enhancement factor E_mod/E_cr (and respectively ε") varies in the range of 1.9–3.9 fold. Here 〖E〗_mod is the amplitude of the local field of the modified plate; E_cr is the amplitude of the local field of a silicon substrate when illuminated by a laser with a wavelength of 635 nm. According to the relation (22), this should correspond to a theoretical increase in the absorbed power by a factor of η^2≈4"–" 15 times.
Direct measurements of the output electrical characteristics in an open-circuit condition demonstrate a clear correlation between an increase in the PVC power generation and an increase in the intensity of the local electromagnetic field due to LSPR and the back scattering of electromagnetic radiation by the surface, as evidenced by the sign of the real part and the corresponding increase in the imaginary part of the complex dielectric constant.
However, despite the significant increase (up to an order of magnitude) in the local absorption of radiation energy expected in theory due to such an increase in the total intensity of electromagnetic radiation, the experimentally measured increase in PVC power productivity is within the range of 9-30%. This discrepancy can be explained by the high localization of the field amplification caused by both plasmon resonance and scattering, which does not spread evenly throughout the volume. Differences between the estimated and measured values may also be related to the structural heterogeneity of the coatings and the surface condition, including inherent and modified defects and morphological features of the PVC.

6 CONCLUSION

The nondestructive optical method for determining the complex dielectric permittivity ε(ω)= ε'(ω) + iε"(ω) of silver nanoparticle-modified silicon surfaces has been developed and experimentally validated. The method is based on analysis of backscattered radiation and enables reconstruction of both real and imaginary components of permittivity without altering the sample structure.
It was demonstrated that the formation of a metallic nanophase leads to a 2–5-fold increase in backscattering intensity, corresponding to a significant modification of the optical response of the system. This behavior is associated with the excitation of localized surface plasmon resonances (LSPR), characterized by the condition ε'(ω) < 0.
The obtained results show that the imaginary part of the dielectric permittivity ε" plays a key role in determining the efficiency of electromagnetic energy absorption. The experimentally observed increase in photovoltaic power (9–30%) correlates with both the enhancement of the local electromagnetic field and the increase in effective dissipative losses in the near-surface region.
Despite the theoretically predicted of high electromagnetic energy absorption, the total efficiency of PVCs' productivity gain remains limited due to localized nature of the LSPR and scattering effects and structural inhomogeneity of the nanoparticle distribution.
The proposed method demonstrates good agreement with reference optical data and can be considered a reliable tool for diagnostics and optimization of plasmonic coatings in photovoltaic and optoelectronic systems.

ACKNOWLEDGMENTS

This research was carried out with the financial support of the Russian Science Foundation within the framework of scientific project No 21-79-30058-П. The study was carried out on the equipment of the Center of collective use of MSUT "STANKIN". and the project Society in the Mirror of Water – Long-Term Strategic Research in the Field of Wastewater Analysis as a Tool for Monitoring Public Health and Environmental Safety, project

code: 401101C229, co-financed by the European Union under the Programme Slovakia 2021–2027.

REFERENCES

[Abu-Thabit 2020] Abu-Thabit, N.Y., Makhlouf, A. Fundamental of smart coatings and thin films: synthesis, deposition methods, and industrial applications. Advances in Smart Coatings and Thin Films for Future Industrial and Biomedical Engineering Applications, 2020, pp. 3-35. DOI: 10.1016/B978-0-12-849870-5.00001-X

[Baker-Jarvis 1993] Baker-Jarvis, J., et al. Transmission/reflection and short-circuit line methods for measuring permittivity and permeability. NIST Technical Note 1355-R., Washington, 1993, 124 p.

[Bohren 1983] Bohren, C.F., Huffman, D.R. Absorption and Scattering of Light by Small Particles. Wiley, 1983, 554 p.

[Car 2025] Car, J., Pietrzak, K., Krstulovic, N. Determination of dielectric functions of colloidal silver nanoparticles. Applied Physics A, 2025, Vol. 131, 1028. https://doi.org/10.1007/s00339-025-09121-6

[Catchpole 2008] Catchpole, K.R., Polman, A. Design principles for particle plasmon enhanced solar cells. Applied Physics Letters, 2008, Vol. 93, 191113. https://doi.org/10.1063/1.3021072

[Chen 2004] Chen, X., Grzegorczyk, T.M., Wu, B.-I., Pacheco, J., Kong, J.A. Robust method to retrieve the constitutive effective parameters of metamaterials. Physical Review E, 2004, Vol. 70, No. 1, 016608. https://doi.org/10.1103/PhysRevE.70.016608

[Grigoriev 2023] Grigoriev, S.N., et al. Electrophysical Technologies: Plasma-Electrolytic Chemical-Thermal Treatment of Materials. Moscow: Stankin, 2023, 366 p.

[Gulyaev 2022] Gulyaev, P., et al. Particle and Particle Agglomerate Size Monitoring by Scanning Probe Microscope. Applied Sciences, 2022, Vol. 12, No. 4. DOI: 10.3390/app12042183

[Husain 2021] Husain, H., Hazdra, Z., Kudlacek, J., Kuchar, J. Risk factors for B4C composite utilization in tribological processes. In: Metal 2021 - 30th Anniversary International Conference on Metallurgy and Materials, Conference Proceedings. Brno, 26-28 May 2021. Ostrava: Tanger Ltd., 2021, pp. 801-806. ISSN 2694-9296. ISBN 978-80-87294-99-4. DOI: 10.37904/metal.2021.4186

[IEC 60904-1 2006] IEC 60904-1. Photovoltaic devices - Part 1: Measurement of photovoltaic current-voltage characteristics. Geneva, Switzerland, 2006.

[Kadochkin 2013] Kadochkin, A.S., Shalin, A.S., Maslov, N.A., Nizametdinov, A.M. Non-absorbing metamaterial with dispersion of the effective refractive index. Physical and mathematical sciences, 2013, Vol. 4, pp. 119-132. Available at: https://www.mathnet.ru/rus/ivpnz382

[Krenicky 2024] Krenicky, T., Goncharov, O.Y., Kuchar, J., Sapegina, I.V., Kudlacek, J., Faizullin, R.R., Korshunov, A.I., Cerny, D. Chemical Vapor Deposition of Tantalum Carbide in the TaBr5–CCl4–Cd System. Coatings, 2024, Vol. 14, No. 5, 547. DOI: 10.3390/coatings14050547

[Krit 2024] Krit, B.L., et al. Development of a Method for Controlling the Parameters of Photovoltaic Converters. Opt. Spectrosc., 2024, Vol. 132, pp. 64-67. https://doi.org/10.1134/S0030400X24700346

[Krit 2020] Krit B.L., et al. The Application of Nanocluster Coatings for Modification of Receiving Surface of Thermal-Photoelectric Energy Converters. Surface Engineering and Applied Electrochemistry, 2020, Vol. 56, No. 1, pp. 100-104. DOI: 10.3103/S106837552001010X

[Krupka 2021] Krupka, J. Microwave Measurements of Electromagnetic Properties of Materials. Materials, 2021, Vol. 14, 5097. DOI: 10.3390/ma14175097

[Kubota 2024] Kubota T., et al. Optical Properties and Applications of Diffraction Grating Using Localized Surface Plasmon Resonance with Metal Nano-Hemispheres. Nanomaterials, 2024, Vol. 14, No. 19, 1605. https://doi.org/10.3390/nano14191605

[Kuric 2022] Kuric, I. et al. Approach to Automated Visual Inspection of Objects Based on Artificial Intelligence. Applied Sciences, 2022, Vol. 12, Issue 2, DOI: 10.3390/app12020864

[Luukonen 2011] Luukkonen, O., Maslovski, S.I., Tretyakov, S.A. A Stepwise Nicolson–Ross–Weir-Based Material Parameter Extraction Method. IEEE Antennas and Wireless Propagation Letters, 2011, Vol. 10, pp. 1295-1298. https://doi.org/10.1109/LAWP.2011.2175897

[Mascenik 2024] Mascenik, J., Coranic, T., Kuchar, J., Hazdra, Z. Influence of Selected Parameters of Zinc Electroplating on Surface Quality and Layer Thickness. Coatings, 2024, Vol. 14, No. 5, 579. https://doi.org/10.3390/coatings14050579

[Mcoyi 2025] Mcoyi, M.P., Mpofu, K.T., Sekhwama, M., Mthunzi-Kufa, P. Developments in Localized Surface Plasmon Resonance. Plasmonics, 2025, Vol. 20, pp. 5481-5520. https://doi.org/10.1007/s11468-024-02620-x

[Miglierini 2006] Miglierini, M., et al. Magnetic microstructure of NANOPERM-type nanocrystalline alloys. Physica Status Solidi (B), 2006, Vol. 243, Issue 1, pp. 57-64. DOI: 10.1002/PSSB.200562446

[Mogilnaya 2020] Mogilnaya, T.Yu., Vasiliev, A.M., Pagava, L.L., Kukushkin, D.Yu. The development of a mathematical model of the propagation of radiation in metal nanoclusters in order to determine the possibility of controlling their properties by the SBS method. Journal of Physics: Conference Series, 2020, Vol. 1515, 022020. https://doi.org/10.1088/1742-6596/1515/2/022020

[Mogilnaya 2021a] Mogilnaya, T.Yu., et al. Evaluation the Influence of Impurities on the Occurrence of a Local Surface Plasmon Resonance Effect. Surface Engineering and Applied Electrochemistry, 2021, Vol. 57, No. 5, pp. 567–571. DOI: 10.3103/S1068375521050094

[Mogilnaya 2021b] Mogilnaya, T.Yu., et al. The effect of nonmetallic impurities on the occurring of the surface plasmon resonance at the deposition of nanocluster coatings onto the surface of photo-electric converters. Optics Communications, 2021, Vol. 494, 127065. https://doi.org/10.1016/j.optcom.2021.127065

[Nicolson 1970] Nicolson, A.M., Ross, G.F. Measurement of the intrinsic properties of materials by time-domain techniques. IEEE Transactions on Instrumentation and Measurement, 1970, Vol. 19, No. 4, pp. 377-382. https://doi.org/10.1109/TIM.1970.4313932

[Ordal 1983] Ordal M.A., et al. Optical properties of the metals Al, Co, Cu, Au, Fe, Pb, Ni, Pd, Pt, Ag, Ti, and W in the infrared and far infrared. Applied Optics, 1983, Vol. 22, No. 7, pp. 1099-1120. DOI: 10.1364/AO.22.001099

[Parveen 2025] Parveen, F., et al. Silver Nanoparticles in Plasmonic Solar Cells: A Review. ES Materials & Manufacturing, 2025, Vol. 29, 1548. https://doi.org/10.30919/mm1548

[Preston 2021] Preston, A.S., Hughes R.A., Dominique N.L., Camden J.P., Neretina S. Stabilization of Plasmonic Silver Nanostructures with Ultrathin Oxide Coatings Formed Using Atomic Layer Deposition. Journal of Physical Chemistry C, 2021, Vol. 125, No. 31, pp. 17212-17220. DOI: 10.1021/acs.jpcc.1c04599

[Ramezani 2023] Ramezani, M., Mohd Ripin, Z., Pasang, T., Jiang, C.-P. Surface Engineering of Metals: Techniques, Characterizations and Applications. Metals, 2023, Vol. 13, No. 7, 1299. DOI: 10.3390/met13071299

[Rothwell 2016] Rothwell, E.J., Frasch, L.L. Analysis of the Nicolson-Ross-Weir Method for Measuring the Permittivity and Permeability of Materials. Progress In Electromagnetics Research, 2016, Vol. 157, pp. 31-47. https://doi.org/10.2528/PIER16072705

[Saga 2011] Saga, M. et al. Contribution to Modal and Spectral Interval Finite Element Analysis. Vibration Problems ICOVP 2011, Vol. 139, pp. 269-274. DOI: 10.1007/978-94-007-2069-5_37

[Saito 2021] Saito, N., et al. Effect of chemically induced permittivity changes on the plasmonic properties of metal nanoparticles. Communications Materials, 2021, Vol. 2, 54. DOI: 10.1038/s43246-021-00159-6

[Schenk 2018] Schenk T., et al. Physical Approach to Ferroelectric Impedance Spectroscopy: The Rayleigh Element. Physical Review Applied, 2018, Vol. 10, 064004. DOI: 10.1103/PhysRevApplied.10.064004

[Suslov 2008] Suslov, A.G. Surface Engineering of Parts. Moscow: Mechanical Engineering, 2008, 320 p.

[Taha 2024] Taha, B.A., et al. Plasmonic-enabled nanostructures for designing the next generation of silicon photodetectors: Trends, engineering and opportunities. Surfaces and Interfaces, 2024, Vol. 48, 104334. DOI: 10.1016/j.surfin.2024.104334

[Tolmachev 2017] Tolmachev, V., Zharova, Y. Study of the optical properties of silver nanoparticle layers and Si-based nanostructure layers. Phys. Status Solidi B, 2017, Vol. 254, 1600758. DOI: 10.1002/pssb.201600758

[Weir 1974] Weir, W.B. Automatic measurement of complex dielectric constant and permeability at microwave frequencies. Proceedings of the IEEE, 1974, Vol. 62, No. 1, pp. 33-36. DOI: 10.1109/PROC.1974.9382

[Yang 2026] Yang, Y., et al. Inverse-designed plasmonic biosensors with LSPR-SPP coupling in silver nanostructures. J. of Nanobiotechnology, 2026, Vol. 24, 58. DOI: 10.1186/s12951-025-03930-w

[Yelwa 2024] Yelwa, J.M., Musa, H. Innovative smart coatings: advancing surface protection and sustainability across industries. Academia Nano: Science, Materials, Technology, 2024, 1. https://doi.org/10.20935/AcadNano7343

[Yu 2017] Yu, P., et al. Effects of Plasmonic Metal Core-Dielectric Shell Nanoparticles on the Broadband Light Absorption Enhancement in Thin Film Solar Cells. Scientific Reports, 2017, Vol. 7, 7746. https://doi.org/10.1038/s41598-017-08077-9

[Zharova 2019] Zharova, Y., Ermina, A., Pavlov, S., Koshtyal, Y., Tolmachev, V. Spectroscopic Characterization of Silicon Wire-Like and Porous Nanolayers in the Process of Metal-Assisted Chemical Etching of Single-Crystal Silicon. Phys. Status Solidi A, 2019, Vol. 216, No. 17, 1900318. DOI: 10.1002/pssa.201900318

CONTACTS:

BORIS LVOVICH KRIT, TATIANA YUREVNA MOGILNAYA, NIKITA ALEXANDROVICH PETELIN, YAROSLAV VALERYEVICH DOLGUSHIN
Moscow Aviation Institute (National Research University), Moscow 125993, RF

MAROS SOLDAN, Prof. Ing. PhD.
Slovak University of Technology in Bratislava, Faculty of Materials Science and Technology in Trnava, Institute of Integrated Safety
Jana Bottu 2781/25, 917 24 Trnava, Slovakia
E-mail: maros.soldan@stuba.sk

SVETLANA IVANOVNA SOLOMENNIKOVA, BORIS ANATOLYEVICH YAKIMOVICH
Sevastopol State University, Sevastopol 299053, Crimea

LEONID YURYEVICH YUFEREV
Federal Scientific Agroengineering Center VIM, Moscow 109428, RF

NATALYA VLADISLAVOVNA MOROZOVA
Moscow State Technological University STANKIN, Moscow 127055, RF